Determination of interfacial shear strength in continuous fibre composites by multi-fibre fragmentation

Determination of Interfacial Shear Strength in Continuous Fibre Composites by Multi-Fibre Fragmentation: A Review

by

Edward D. McCarthy[1*], Constantinos Soutis[2]

1. School of Engineering, The University of Edinburgh, Sanderson Building, Kings Buildings, Edinburgh, EH9 3FB, UK.

2. School of Materials, The University of Manchester, Oxford Road, Manchester, M13 9AX, UK.

*Corresponding Author: Email address: ed.mccarthy@ed.ac.uk

This research did not receive any specific grant from funding agencies in the public, commercial, or not-for-profit sectors.

Abstract

In a fibre-reinforced polymer matrix composite (PMC), the function of the fibre is to bear the applied load that is transferred via shear stresses through the fibre-matrix interface from the polymer matrix. The fibre absorbs stress by progressively fragmenting along its axis until a critical fibre fragment length is realized. After this no further fragmentation is possible, the fibre is said to be "saturated" in stress, and it provides no strengthening upon further deformation. A critical and intrinsic material property of the composite that determines the failure of the fibre is the interfacial shear strength (IFSSh) between matrix and fibre.

This review presents the multi-fibre fragmentation technique (MFFT) and Laser Raman Spectroscopy (LRS) which are used for fibre-matrix interface testing. The limitations of MFFT are summarised and ideas for improvement are proposed.

The key findings of this review are: 1) MFFT equipment and protocols vary considerable and require standardisation. 2) Existing models for stress transfer between fibres rely on geometrical models that do not capture the material properties or the constitutive models of the transmitting matrix. Comprehensive constitutive matrix stress transfer models are needed.

Current MFFT models do not incorporate terms for matrix vibration as a function of fibre fracture shock. It is clear that more work can also be done to characterize microcomposite systems in compression, at various

angles to the fibre axis, and under various combinations of cyclic loading, but arguably such work should be pursued after the uniaxial tensile fibre fragmentation problem has been better understood.

Keywords: interfacial shear strength; multi-fibre fragmentation; composites; Raman spectroscopy.

Note: IFSS: interfacial shear stress.

IFSSh: interfacial shear strength.

1.0 Introduction

Currently, there is a range of diverse techniques for determination of interfacial shear strength at a fibre-matrix interface: A) direct-contact fibre pull- or push-out separation techniques, and B) indirect non-contact methods that measure fibre-matrix interfacial behaviour without separating the fibre from the matrix. The latter techniques include fibre fragmentation that is used with or without Raman spectroscopy or photoelastic photography, to monitor fibre strain and matrix shearing *in-situ* during specimen deformation. Fibre pull- and push-out techniques have been well documented and modeled [1-6] and are not the subject of this review. However, it should be emphasized that fibre pull-out and push-out techniques require a portion of a reinforcing fibre to be located outside the resin of interest, a condition not observed in application. Fibre fragmentation, by contrast, is a technique which studies the behaviour of the fibre-matrix interface for a fibre that is completely embedded in a matrix, and for that reason it has special relevance as a technique capable of more accurately capturing interface behaviour, without the complication of a fibre/resin/air interface to consider.

The theoretical history of the single fibre fragmentation test has been well documented, i.e., the development of the Cox and Kelly Tyson shear lag models and others. [7], [8]. These theories describe axial fibre strength distribution, and provide statistical approximations for critical fibre fragment length using mean fragment length data. There are also various local load-sharing models that described stress transfer between a fragmented fibre and its intact neighbors. [9], [10]. All of these models are either theoretically conceived, based on elementary force balances on the fibre-matrix interface, or on statistical expressions which approximate variables such as critical fibre fragment length that are currently inaccessible to direct measurement. However, at present, many of these models are based on simplifying assumptions about matrix deformation, interface debonding, and supposed linear-elastic or elastic-perfectly-plastic mechanical behavior of the composite matrix. This is principally because constitutive models for the mechanical behaviour of amorphously structured thermoset matrices are under-developed by comparison with metals, which possess a degree of long-range order at the atomic level, so that metallic behaviour under applied loads may be described with more accuracy than that of thermoset matrices.

In this review, the focus is on the history and development of experimental fragmentation techniques that have been devised to interrogate the fibre-matrix interface in polymer composites, and describe significant historical data derived from these. The main aim of these techniques has been, and remains, to achieve a

robust protocol for the measurement of interfacial shear strength (IFSSh). Ideally, IFSSh should be measured in a direct manner. However, in practice, most techniques of the past fifty years have concentrated on the measurement of critical fibre fragment lengths at fibre stress saturation as a faster route to the calculation of IFSSh, rather than on direct measurement of the latter, which has proven intractable. This has necessitated the development of theoretical and statistical models to improve confidence in the relationship between mean fragment length actually measured in these tests, the notional critical fibre length at saturation, and the real interfacial shear strength of the fibre-matrix interface. However, the necessary mathematical relationships between these quantities are heavily dependent on experimental data for their validation; particularly, as many of the qualitative predictions of the purely mathematical, non-statistical models are not properly representative of real interfacial behavior, which will be discussed in this review by examination of historical data.

The experimental techniques described in this review can be divided in two categories: a) qualitative techniques such as laser Raman spectroscopy (LRS) that are used to visualize or otherwise monitor behaviour at the fibre-matrix interface during a fibre-matrix shear or debond event and b) mechanical fibre fragmentation tests under applied uni-axial tension. It is hoped that this review will present a concise summary of techniques and data on IFSSh, and may help direct future research efforts in the most productive direction possible to accelerate the development of a robust methodology, and ultimately a standard, for the determination of IFSSh. Ultimately this could be used to determine the interlaminar shear strength of a unidirectional laminate, but further research will be required.

2.0 Laser Raman Spectroscopy (LRS) for IFSS Determination

Fibre fragmentation tests have long been supported by Laser Raman Spectroscopy (LRS) [11]. Tuinstra and Koenig [12, 13] first identified the Raman vibrational modes of graphitic carbon fibres in 1970. Then, Mitra et al [14] established the measurable stress dependence of a Raman peak for polydiacetylene monocrystals in 1977, while Penn and Milanovitch (1979) [15] adopted this approach to measure strain dependence of poly(p-phenylene terephthalamide fibres (PPT, Kevlar 49). Galiotis et al. (1984) were the first to use LRS to measure the strain dependence of Raman peaks in polydiacetylene fibres rather than crystals [16], and also conducted a study on the Raman response of a crystalline urethane resin system to tensile strain [17]. After this, (1987-88), the Raman spectrum response of intermediate- and high-modulus carbon fibres under uniaxial tension was also analysed and compared using LRS by Robinson et al. & Galiotis et al. [18, 19]. This work was followed by a series of papers by Galiotis and co-workers studying fibres embedded in polymer resins to determine stress transfer characteristics at the fibre-matrix interfaces of these composites [20-27]. A contemporary 1990s review of the work on fibrous composites of this period is provided by Galiotis et al. (1999), [28].

The basis of the Raman measurement method is the strain- and stress- dependence of certain vibrational modes of molecules in the reinforcing carbon fibres. Thus, Raman spectroscopy can be used to measure fibre stress and strain with a spatial resolution of 1 μm. In addition, the strain- and stress-dependence of key graphitic vibration modes in carbon fibres is highly linear, which facilitates more accurate measurements of strain and stress using this technique. The fundamentals of the strain dependence of LRS vibration modes is well explained by Frank et al [29] who describe the use of LRS as a stress-sensor for both graphene and carbon fibres, while Anagnostopoulos et al. [30] have exploited the phonon stress sensitivity of carbon to characterize fibre matrix interfaces at different temperatures.

The key advantage of Raman-sourced fibre strain data is that the normal stress function $\sigma_f(x)$ along the fibre axis can be determined directly by experiment, so that neither the Kelly-Tyson nor shear lag models are required to calculate it. An immediate consequence of this is that an independent experimental verification of the accuracy of shear lag models and their underlying assumptions is possible using LRS.

Once the axial shear stress distribution has been determined by experiment, it can be directly converted to the corresponding axial shear stress distribution using the following equation, c.f. Galiotis et al., [28]

$$\tau(x) = -\frac{r}{2}\left(\frac{\partial\sigma}{\partial x}\right)_T \quad (1)$$

Here, τ(x) is the interfacial shear stress distribution, r is the radius of the fibre, σ is the axial tensile stress distribution in the fibre, and the expression is written for a constant temperature, T. A 1995 review by Schadler et al. [21] describe the application of this methodology to a variety of systems including carbon fibre microcomposites. One of the first discoveries made by Melanitis et al. [22] using LRS was that the constant-axial-IFSS assumption of the Kelly-Tyson model was only approximately justified for one system tested. This was a DGEBA/TETA matrix (MY750) with an embedded, untreated high modulus carbon fibre (HMU) (Figure 1), (Schadler et al. [21]). It was found that that this type of fibre had a weak fibre interphase layer in the vicinity of both fibre fragment ends. Such a layer resulted in debonding of the interface in the immediate vicinity of either fibre break, so that the interfacial shear stress could not develop gradually from zero (or a negligible value) at the fibre end to a maximal value towards the fibre centre, due to low or no interfacial shear stress transfer through the partially or fully debonded fibre end regions (IFSSh ~ 6 MPa). However, where carbon fibre surfaces were adequately treated to facilitate the formation of a well-bonded interface (IFSSh ~ 40 MPa), a much greater Raman-measured strain-increase was detected from either fibre end, consistent with Cox-type stress-transfer models (See IMD / MY-750 and HMS / MY-750 plots, Figure 1). However, unlike the Cox shear lag model, Raman-derived IFSS profiles for well bonded interfaces (e.g. IMD and HMS systems in Figure 1) observed maxima not at the absolute fibre ends, but rather at a certain distance from either end of the fibre. The use of LRS to demonstrate this fundamental property of interfacial shear stress distribution along a fibre fragment with a reasonably intact interface was one of its earliest and greatest successes, and agreed well with the models of McCartney [31] and Whitney and Drzal, [32] as these workers' model predicted an IFSS maximum some small distance from the fibre end. The second main insight provided by LRS was that IFSS axial profiles were highly strain-sensitive In Figure 2, Melanitis et al., [22], a definite change in the characteristic shape of the IFSS curve is observed as strain transitions from 1.2% to 1.4%, something not at all anticipated by any shear lag model. In the same study, the authors presented IFSSh (a plot of the maximum IFSS values in each measured Raman profile) at different fibre axial strains (See Figure 3), [23]. For this particular fibre-matrix system, it is notable that the maximum IFSS recorded is at an intermediate strain, above which the maximum IFSS tends to decrease, which becomes statistically significant above 4% strain. Of course, such measurements would

require to be made in conjunction with measurements of mean fibre fragment length, since one condition for determination of IFSSh is stress saturation of the fibre.

Overall Melanitis et al. [22,23] demonstrated how crucial it is to make a qualitative determination of bond quality in the fibre-end regions and to take account of applied strain effects before uncritically applying the assumptions of any theoretical model to describe the axial interfacial shear stress function.

For comparison, the matrix shear yield stress τ_m was estimated using the von Mises and Tresca yield criteria. These equated τ_m to (σ_m / $\sqrt{3}$) and (σ_m / 2) respectively, giving values of 37.5 and 32.5 MPa. Here, σ_m is the maximum matrix stress. Thus, the IFSSh value for the IMD composite (~40 MPa) was significantly higher than the Tresca matrix yield stress, whereas the IFSSh value for the HMS-composite was practically equivalent to τ_m. This indicated that the IMD composite would yield in the matrix first rather than along the interface, whereas the HMD composite *could* debond along the interface first. However, when the Kelly-Tyson model (Eqn. 2) is used to calculate IFSSh, the K-T IFSSh-value is only ca. half the Tresca matrix yield stress. If the LRS-measured IFSSh is assumed to be more accurate, this demonstrates a clear contrast between credible experimental data for IFSSh and a classical theoretical model for its calculation, where LRS-measured IFFSh tends to be twice the K-T IFSSh, [22]. Eqn. 2 is the fundamental expression for the Kelly Tyson model, [8].

$$\frac{l_c}{d_f} = \frac{\sigma_f(l_c)}{2\tau} \approx \frac{\overline{\sigma_f}}{2\tau} \qquad (2)$$

Here, l_c is critical fibre fragment length, σ_f is the fibre normal stress as a function of l_c, $\bar{\sigma}$ is the mean fibre tensile stress, and τ is the interfacial shear strength.

The decrease of IFSSh with increasing fibre tensile modulus is consistent with data derived for interlaminar shear strength (ILSS) for carbon fibre composites, which also show decrease of ILSS with increase in carbon fibre modulus. However, the LRS data contradicts the trend predicted by the shear lag models, where the axial IFSS profile of the fibre is predicted to increase with fibre modulus, thus predicting an IFSSh value (the maximum of the IFSS curve) that is too high, implying sooner interface failure than is actually the case, [21]. This further highlights a structural inability of the shear lag models to account for the effect of fibre tensile modulus on interfacial shear strength. Thus, quantitative deficiencies in both the shear lag and Kelly-Tyson models are revealed when using LRS to measure IFSSh for composite systems.

Galiotis et al. [16] produced Raman data for Kevlar 49 (PPT) fibres embedded in epoxy, which suggested significantly different interfacial behaviour to that of the carbon fibre / epoxy system they tested (HMS/MY750). Firstly, IFSS for the carbon epoxy system was usually near zero at fibre ends regardless of applied strain because of near total debonding near the fibre break, and the carbon fibre system also featured a significant load transfer length indicative of partial (but not total) debonding. By contrast, the Kevlar/927 epoxy system mostly showed high IFSS near fibre ends indicative of a relatively intact interface, further demonstrating the significant descriptive power of LRS to describe different fibre-matrix interface behavior for different fibre interface bond states.

In other work, Jahankhani and Galiotis [26] noticed that the strain transfer profiles of a Kevlar/DGEBA/TETA system followed a qualitative trend described by the shear lag models. However, they also observed an increase of the critical length, l_c with strain, which is not predicted by these models. This is because the shear lag models assume that both the matrix and fibre behave elastically during loading i.e. the ratio G_m/E_f remains constant during mechanical loading. However, in reality this ratio can change, even at low strain for some low strength matrices, because the matrix is viscoelastic and also because of the operation of strain-hardening during tensile loading of aramid fibres.

Some of the most recent work on LRS was that of Jin et al. [33] in 2014, where the authors studied the coating of two types of carbon fibres (the first: Toray M46J, high modulus; the second: Toho-Tenax-J, low-modulus) with two types of carbon nanotubes, one HiPCO (high pressure, carbon monoxide) and the second carboxylated. The authors derived interfacial shear stress axial profiles from the primary measured strain profiles that clearly indicated the presence of fibre breaks due to an absence of strain. Secondly, the profiles largely conformed to those predicted by Nairn's shear lag model, [34], but only where debonding was not present. Nairn's model has the advantage of being heavily dependent on fibre and matrix volume fractions as well as the fibre and matrix elastic moduli, which are all accessible via macroscopic mechanical measurements. However, Nairn's model is written for a fibre embedded in an 'infinite' matrix, and so could not be formally applied to the situation of multiple fibres in proximity (parallel). In addition, the authors demonstrate very clearly that the Kelly Tyson model predicts stress development 'slopes' that are much steeper than those measured via LRS. Thus, IFSSh measured by Raman typically exceeds that calculated using critical fibre fragment lengths and the Kelly-Tyson equation. Lastly, the stress development lengths at either end of fragments remain largely constant with increasing strain, diverging from the Kelly-Tyson

model which predicts that both will lengthen with increasing fragment tensile strain and implying that the ratio G_m/E_f remains practically constant throughout the fragmentation process (in contrast to the results of Jahankhani and Galiotis [26], proving that qualitative IFSS distributions vary with material systems.

Overall, in addition to its quantitative accuracy in describing IFSS, an experimental advantage of the LRS method is its flexibility of application. Normally, in tensile techniques for determination of IFSS, matrix strain-to-failure should ideally be two to three times greater than that of the fibre to facilitate the measurement [34]. However for Raman-active fibres, LRS can be used for matrix/fibre strain-to-failure ratios much smaller than this [22], which is more representative of systems used in engineering applications.

2.1 Use of Raman to study Inter-Fibre Stress Transfer

Raman techniques have also been used to study the lateral stress transfer from broken fibres to intact fibres, (Grubb *et al.* [9]). Here, the authors formulated various epoxy-based composites with 1) Nicalon silicon carbide fibres of 15 μm diameter, 2) carbon AS4 (7.6 μm) 3) carbon Fortafil (7.6 μm) and 4) Kevlar-49 fibres (15 μm). The AS4 was the only fibre supplied with an epoxy-compatible sizing; the others were unsized as received and were not treated further by the authors.

Two epoxy-resin mixtures were used: 1) Epoxy I; DER 331 (diglycidyl epoxide of bisphenol A) neat, cured with DEH 26 (tetraethylene diamine) 2) Epoxy II; a 70:30 mass ratio of DER 331 to DER 732 (polyglycol diepoxide). The latter mixture had lower modulus because DER 732 had the effect of a diluent or flexibilizer, and was also cured with DEH 26. Specimens were cured at room temperature for 24 h and for 3 h at 80 °C in silicone rubber moulds, according to a procedure described by Drzal et al. [35], for single and multi-fibre fragmentation tests, respectively. Fibre fragmentation tests were then performed.

Raman spectra of Kevlar monitor fibres placed adjacent to embedded fibres were obtained in the following manner; a 514 nm Argon laser and spectrometer with grating number of 1800 / mm, was focused on specimens through a 10x magnification microscope, creating a focus spot of 10 μm in diameter. Each specimen was stretched initially on a tensile stage to introduce one break only in the embedded fibre. *Prior to the Raman measurement*, the photoelastic pattern of stress concentrations around the fibre at this break was recorded using a polarization microscope. Then the strain stage was put under the Raman objective, which was equipped with both a load cell and displacement monitor. A maximum incident laser power of

2 mW was then directed on the fibre to avoid inducing degradation damage in the Kevlar monitor fibre, and the Raman shift in key signals of the fibre spectrum was recorded as strain was applied.

In general, Epoxy I showed 10-15 % stress relaxation in contrast to Epoxy II, which showed little to none; therefore, each specimen was allowed to remain at a given load for a minimum of 0.5 h before any shifts were recorded to allow such relaxations to be exhausted. This process was applied at each successive strain level applied. After the relaxation period, the stress profile along the entire length of the fibre was calculated from the corresponding Raman shift profile. Stress concentration factors (SCF or K_c) adjacent to breaks were calculated by taking the ratio of Raman shifts at fibre breaks to those recorded relatively far from breaks using Eqn 3

$$K_c = 1 + \frac{[W_1 - W_2]}{|W_1 - W_0|} \quad (3)$$

Here, W_1 and W_2 are the peak Raman wavenumbers for the off-break and at-break fibre positions, respectively, whereas W_0 is the peak wavenumber at no external load. Thus, at two strain levels of 2.65 and 3.25 %, the Nicalon fibre stress concentration was 1.4 ± 0.12 and 1.45 ± 0.09, respectively. The authors also determined from the Raman stress profiles that the load transfer length for a typical Nicalon fibre break was approximately 230 μm. This was a value, which accorded well with the corresponding birefringence measurements for the same specimens.

The authors compared their results with outcomes predicted by shear lag theory. Since, according to the latter, the matrix bears mostly shear stress and little tensile stress, most of the tensile stress released upon a fibre break in a three-fibre system should be transferred to the two adjacent intact fibres. The local load sharing model, (LLS) load transfer factor for the system, F = 0.5. This is calculated as $F = K_{LLS} - 1$ via Eqn 4, where K_{LLS} is the stress concentration factor acting on the average load of a bundle of fibres, L, (i.e., $K_{LLS}L$ is the load on an intact fibre adjacent to a broken one, where L is the original load on the broken fibre at point of fracture), r is the number of failed fibres, and n is the number of fibres, Harlow et al. [36, 37].

$$K_{LLS} = \begin{Bmatrix} 1 + \frac{r}{2} & 0 \le r \le n-1 \\ n & r = n-1 \end{Bmatrix} \quad (4)$$

The key assumption of Harlow's LLS is that the bundle of fibres is arranged in a circle with each fibre interacting with precisely two others, e.g., a hexagonal arrangement of fibres without a central fibre contacting the six outside fibres.

Since the Nicalon and Kevlar fibres had equivalent cross-section areas, the calculated stress concentration factor of the system was 1.8. This was somewhat in excess of the actual value of 1.45 derived from the Raman measurements in Epoxy 1, and implied that 56 % (0.45/0.8) of the load borne by the Nicalon fibre was transferred to the two Kevlar fibres, and the remaining 44 % was borne by the matrix. This suggested immediately that matrix axial stress was not negligible, as predicted by shear lag theory, but rather quite significant. Moreover, since the matrix was relatively weak, it was clear that a significant cross-sectional area would be required to bear this axial stress. From the equation $A_m E_m \varepsilon_m = C_f A_f E_f \varepsilon_f$ where $C_0 = 0.44$, the actual ratio of matrix to fibre area was calculated as $(A_m/A_f) = 23$. This meant that the stress displaced from a fibre break could be dissipated into the matrix over at least five fibre radii in Epoxy 1.

However, in Epoxy 2, the situation was somewhat different as the stress concentration in the Kevlar fibres was now lower at 1.36. Accordingly, only half the Nicalon fibre load was transferred to the two Kevlar fibres, and half to the matrix. This means the matrix-to-fibre cross-area ratio above was lower at $(A_m/A_f) = 20$. Similar observations were made for particularities of the other fibres tested. Thus, the laser Raman studies reveal how the matrix transfers load to the fibres, but also experiences substantial axial stress that is not captured by the shear lag models.

The second significant output of such work has been its ability to quantify the inter-fibre stress transfer distance for individual material systems, and obtain experimental validation of the matrix radius-of-influence parameter, r_m, that appears prominently in many shear lag models. This parameter in turn is relatable to the fibre volume fraction, V_f, of a composite (assuming a relatively homogenized fibre cross-sectional distribution), suggesting a means of tuning V_f to maximize the individual stress transfer capability of the fibre-type as indexed by its critical fragment length.

2.2 Comparison of Models for Interfibre Transfer used to interpret Raman Data

Overall, Grubb's experimental data indicated that a serious deficiency of the shear-lag models was their inability to account for the existence of matrix axial stress. This was verified from their experiments, where a broken Nicalon fibre shed load to its two nearest-neighbour Kevlar fibres, and K_c was calculated, using the Eitan-Wagner model with a value of 1.8. However, K_c measured using the Raman peak shift was only 1.45. This was effective proof that the matrix had to be bearing 44% of the system's overall axial tensile stress, rendering the Eitan and Wagner equation ineffective for use in calculating the load transfer factor F and and the SCF K_c adjacent to fibre breaks. This meant a revised equation was necessary.

Initially, Grubb et al. [9] had used the Eitan and Wagner equation to calculate theoretical stress concentrations based on a fibre ensemble geometry shown in Figure 4, [38]. This model adopts many of the original assumptions used by Cox, i.e., only shear stress in the matrix, perfect bonding at the matrix-fibre interface. Also, the model assumed a three-dimensional radial stress field around the broken fibre despite the fact that the shear-lag models are based on a two-dimensional composite lamina with only a single sheet of parallel fibres. It was also assumed that the shear stress at any point in the matrix is unaffected in the immediate vicinity of neighbouring *intact* fibres. The shear stress at any point in the matrix is thus expressed by Eqn 5.

$$\tau_m(x,r) = \tau_m(x,r)\frac{r_f}{r} \tag{5}$$

If an intact fibre and a broken fibre are in sufficiently close proximity, the extra force borne by the intact fibre, $\pi r_f^2\, d\sigma$, is balanced by the interfacial shear force in a region where the intact fibre intersects the stress field 'radiating' from the break of the broken fibre. This region is defined (Figure 4) by the angle swept from $-\theta_{max}$ to $\theta_{max,}$ by a radius extending from the centre of the intact fibre. Thus, the force balance for this system is given by Eqn 6:

$$r_f d\sigma(x) = \frac{1}{\pi}\int_{-\theta_{max}}^{\theta_{max}} \tau_m[x, r(\theta)] \sin\alpha \; d\theta \; dx \tag{6}$$

Here, r is the distance from the centre of the broken fibre to the surface of the intact fibre, and is a function of θ. Importantly, the term sin α describes the component of the shear force that acts along the interface. By adapting this expression, a second expression for the load transfer occurring *in the plane of the break* (transverse to longitudinal fibre axis) may be written, (Eqn. 7). Specifically, this describes a load transfer factor, F.

$$F = \frac{1}{\pi}\int_0^{\theta_{max}} \frac{d_r cos\theta - 1}{d_r^2 + 1 - 2d_r cos\theta}\, d\theta \tag{7}$$

Here the term $d_r = d_i/r_f$, where d_i is the inter-fibre separation, (centre-to-centre), and r_f is the common radius of both fibres. This integrand can be analytically solved and reduces to the angle ϕ, which is half the angle that the intact fibre subtends at the centre of the broken fibre, (Figure 4). This means that $F = \phi/\pi$. Since the stress concentration factor, K_c is equated to 1 + F, Wagner and Eitan used the integrand of Eqn 7 to write Eqn 8:

$$K_c = 1 + {}^{\sigma}/_{\pi} = 1 + {}^{1}/_{\pi}\, sin^{-1}\left({}^{r_f}/_{d_i}\right) \quad (8)$$

Some important features of this model are that 1) the matrix shear stress decreases with 1/r, 2) the area over which the stress acts is proportional to r, and 3) the force applied to the neighbouring fibre over an angular sector dφ is proportional to dφ. A consequence of the latter assumption is that if a broken fibre were surrounded by intact fibres, all the load would be transferred to these fibres upon the formation of a break, regardless of the various distances of the fibres, which seems unlikely in practice. In particular, the fraction of load transferred to a fibre that intercepts an angular sector of 2ϕ is calculated simply as the angle ratio ϕ/π, (i.e. 2ϕ/2π, the fraction of the fibre radial zone occupied by fibres). Furthermore, the term sin α represents the component of stress acting on the interface of the intact fiber. Thus, for any length increment of fibre, dx, the area over which stress acts is calculated as r.dx.dϕ/sin α. This means the stress applied is independent of the angle α itself, which represents the orientation of the interface.

One assumption of the model is that *radial* shear stresses in the matrix are unaffected by the presence of fibres, i.e., that only axial matrix shear is observed (not sustained in practice). Thus, if more than one fibre breaks, (i.e., N fibres) the maximum stress concentration is expressed by Eqn. 9:

$$K_c = 1 + {}^{1}/_{\pi} \sum_{n=1}^{N} sin^{-1}\left({}^{r_f}/_{nd_i}\right) \quad (9)$$

According to this model, the excess load on any intact fibre is unaffected by the presence or absence of other intact fibres, and can only be influenced by load transfer from one or more broken fibres. Furthermore, the total load at each fibre cross-section of the composite in this two-dimensional composite model is not constant. Thus, if only two fibres are in proximity and one breaks, the intact fiber will carry only 1/6 the tensile load shed by the broken fiber. The rest of the load "disappears" as the matrix is assumed to experience infinite shear, an assumption not sustainable in practice as matrices always bear some tensile stress. When the model of Eitan and Wagner is applied to a closely-packed two-dimensional fibre array, the extra loads transferred to the intact fibres sum to unity after the first five intact fibres on either side of a broken fibre.

Grubb et al. [9] made changes to the E-W model as they held it was insufficient to model results obtained from their LRS technique. This was because it included a number of unsustainable assumptions. Firstly, it assumed that the excess load on an intact fibre was unaffected by the presence or absence of neighbouring intact fibres, a prediction not upheld by results of Grubb et al. [9]. Secondly, it asserted that the matrix bore

no tensile stress, only shear stress, which was also disproved by Grubb et al. (c.f. beginning of this section). Arguably, these deficiencies of the Eitan & Wagner model might not have been so well confirmed without the use of the Raman technique.

The Grubb model is based on the same specimen geometry as the E-W model (Figure 5), [9]: Here, the load transfer angle, ϕ, is still defined and d_i is the inter-fibre centre-to-centre distance as in the Eitan-Wagner model. However, they substituted the use of r_f, the intact fibre radius, with r_e, an effective matrix interaction radius (not shown in Figure 4) r_e is defined as the radius beyond which there is no significant stress activity in the matrix induced by a fibre break, a quantity somewhat more difficult to define than the radius of the fibre. This produced modified expressions for ϕ, F, and K_c as per Eqns. 10 to 12.

$$\emptyset = cos^{-1}\left({}^{d_i}/_{2r_e}\right) \tag{10}$$

$$F = {}^{\emptyset}/_{\pi} = {}^{1}/_{\pi}\, cos^{-1}\left({}^{d_i}/_{2r_e}\right) \tag{11}$$

$$K_c = {}^{\sigma(0)}\Big/_{\sigma(\infty)} = 1 + F\left({}^{A_0E_0}/_{A_1E_1}\right) \tag{12}$$

Here, $\sigma(0)$ is the local axial stress acting on the intact fibre at the cross-section of the break, while $\sigma(\infty)$ is the undisturbed fibre axial stress at a point on the same intact fibre at a point far from the break.

$$K_c = 1 + \left({}^{A_0E_0\emptyset}/_{A_1E_1\pi}\right) sin^{-1}\left({}^{r_e}/_{d_i}\right) \tag{13}$$

In these new expressions, they also introduced the fibre cross-sectional areas and moduli for the broken $[A_1, E_1]$ and intact fibres, $[A_0, E_0,]$, respectively, which enabled use of their model for systems with dissimilar fibres (hybrid systems). Where two fibres have different tensile moduli *and* cross-sectional areas, it is assumed that the larger fibre will have a larger interaction radius; presumably, because it has a higher load bearing capacity. In this situation, two stress-interaction radii, r_{e0} and r_{e1} are defined for the broken and intact fibres, respectively. r_e is an analogous parameter to the matrix-radius of stress influence, r_m, of the Cox shear lag model, and ideally it should be measured. On this basis, the area ratio of two separate fibre interaction zones is given by Eqn. 14

$$\left(r_{e0}^2 - r_0^2\right)\Big/_{\left(r_{e1}^2 - r_1^2\right)} = {}^{A_0E_0}/_{A_1E_1} \tag{14}$$

Here, r_0 and r_1 are the radii of the intact and broken and fibres, respectively. This expression does allows values for r_e, to be calculated where the moduli and areas of the two fibre types are known. This alters the expression for the interaction angle, ϕ (Eqn. 15)

$$\emptyset = \cos\left(d_i^2 + r_{e0}^2 - r_{e1}^2 \Big/ 2r_{e0}d_i\right) \quad (15)$$

When the interaction distance is less than $r_{e0}\sin\phi_{max}$, Eqn 16 is used

$$\emptyset_{max} = \sin^{-1}\left(r_{e1} \Big/ r_{e0}\right) \quad (16)$$

F can also be evaluated using the concept of area of overlap rather than angle of interaction, i.e., Eqn 17

$$F = A_{ov} \Big/ \pi(r_{e0}^2 - r_0^2) \quad (17)$$

Lastly, it is also possible to express the stress concentration at any fibre (1), $K_1^{r=R}$ at a significant centre-to-centre distance, R, from a broken fibre, in terms of the stress concentration K_1 at a single fibre break using Equation 18, [28], which relates stress concentration to a normalized interfibre distance (R/r_f), where R is the centre-to-centre distance between adjacent fibres, one of which is intact, the other broken:

$$K_1 = K_1^{r=R}\left[R/r\right]^{-0.14} \quad (18)$$

This relationship, fitted on the basis of LRS measurements of point stresses, showed that there was negligible, (but not zero), influence of a fibre break for (R/r) = 11.

2.3 Observations

As mentioned at the start of this section, the E-W model cannot describe the actual inter-fibre stress transfer as it wrongly neglects matrix axial stress. Grubb's modified model represented an improvement on this. In Table 1, Grubb et al., [9], the stress concentration factors calculated for three hybrid fibre systems are compared with predicted values of three models (local load sharing (LLS), Eitan & Wagner, and two variants of Grubb's replacement model). Of the four predictions, that of Grubb's sector angle interaction zone (SAIZ) model achieved the best fit across all three fibre systems, although the area overlap interaction zone (AOIZ) model also achieved relatively good agreement with data for two of these systems. In contrast, the LLS prediction for the Nicalon/Kevlar fibre system was 24% overestimated, but in a good agreement (3-6% difference) for the other two systems. This was also the case for the E-W model that showed 15% reduced SCF for the Nicalon/Kevlar fibre system when compared to the Raman stress data but better

agreement for the other two systems. However, in contrast to both models, the SAIZ model was closest in predicting K_c for all three composite systems. Nevertheless, significant discrepancies exist between all models and the data, and the deviations between various models and the data remain highly system-dependent indicating that none of the models capture all of the parameters necessary to predict the behavior of different systems: i.e., none of these models can be described as a universal model for fibre stress transfer at time of writing.

Overall, it is clear that geometrical models for inter-fibre stress transfer have developed to a fair level of quantitative accuracy, allowing useful data reduction from measurements such as MFFT deployed with LRS. However, by their very nature, they are geometrically constructed and are heavily reliant on the assumption that forces are uniformly transmitted in direct lines, or within definitely described areas defined by angles. As such, they are 'line-of-sight' models only, and are not constitutive models that are derived from constituent material properties, apart from elastic modulus. Thus, there is no provision to calculate a stress transfer efficiency over these areas; it is simply assumed that this efficiency will be 100% if fibres are 'visible to each other'. A comprehensive model would retain the geometrical characteristics of these models, but would also be constructed with a better understanding of the mechanisms of load-transfer through a given polymer matrix, incorporating properties such as fibre Young's modulus and fracture toughness.

3.0 Multi Fibre Fragmentation Test (MFFT)

Stress transfer between fibres is an important area of study in the micromechanics of fibre arrays, particularly in the context of unidirectional lamina. The theoretical treatment of such systems has been discussed elsewhere [39]. Here, we describe the history and development of multi-fibre fragmentation test (MFFT) protocols designed to interrogate fibre-fibre interactions in a two-dimensional unidirectional lamina. Note that studies presented are mostly restricted to discussion of parallel fibres in one plane.

3.1 MFFT Test Protocols

MFFT protocols tend to closely resemble single fibre fragmentation test (SFFT) ones, apart from the configuration of testing frames and equipment, which are modified to achieve consistent inter-fibre spacings. They have been tested over a period of many decades, [38, 39], with numerous techniques for alignment and embedding of these fibre arrays, [40-43]. Usually, the challenge for these techniques has

been the successful embedding of fine, brittle fibres at consistent inter-fibre distances within a matrix, which requires curing, and which shrinks after the fibres have been tensed and mounted in the mould.

In an early version of MFFT (1964), Rosen [44] used prepeg tapes with large fibre volume fractions (~60%) to create such specimens and make qualitative observations and measurements of fibre-breaks in close bundles. Between 92-94 glass fibres of mean diameter 0.127 mm were arranged in parallel arrays and embedded in epoxy plates with dimensions of 12 x 25 x 1.5 mm. Notably, the fibre diameter in these tests was on average five times the inter-fibre spacing of the adjacent fibres. These were tensed along the fibre axis to their ultimate failure load (493-556 N). They discovered that the first breaks were observed at 50% of ultimate load and 130 breaks were observed at ultimate failure representing a linear break density of 5.2 mm^{-1}. Wadsworth and Spilling, [46] pursued a different method by placing dry fibres on parallel linear arrays of pins, rotated at equal rates to achieve the desired fibre tension and inter-fibre separation prior to embedding the tensed fibre system in resin and curing (Schematic illustrated in Figure 6). Nevertheless, the inter-fibre distances achieved were too random for significant conclusions to be drawn from their study. Furthermore, the curing method of these and many other microcomposite systems is different to those used industrially (e.g., autoclave curing), which may result in resin properties different to those of full-scale composite parts produced commercially. Nevertheless, properly controlled inter-fibre spacing can be used to mimic fibre volume fractions that would be achievable industrially, and since the value of the latter tends to dominate fibre-axis composite properties, the effect of differences in matrix shear yield strength and other resin properties may not sufficiently distort the transferability of the analysis from a microcomposite to a full-scale composite part at the sub-tow scale. One caveat to this would be the situation where the matrix yield strength of an under-cured matrix switched from being greater than the interfacial shear strength, to being less than it; however, typical matrix yield strengths (ca. 80 MPa, [46]) are usually far higher than IFSSh (20-60 MPa, [47]), so this will rarely occur.

More controlled embedding of parallel fibres in monolayer epoxy films (microcomposites) was described by Steenbakkers & Wagner, [48], and tensile tests were performed for a variety of Kevlars- and E-glass/epoxy microcomposites to relate strength and modulus properties to closely controlled volume fractions. Gulino and others [49, 50] improvised a three-fibre composite system by pulling the fibres through a fine mesh in order to more closely control fibre-fibre distance. However, this method was difficult

447 and tedious to perform, resulting in too few samples being prepared in the study to develop statistically
448 significant results.

449 By contrast, Wagner & Eitan, [38] and Steenbakkers & Wagner, [48], used a fibre spacing pin-array system,
450 but on this occasion they not only placed fibres between pin arrays, but also rotated the arrays to deliver
451 more accurate and reproducible inter-fibre distances in the ultimate composite specimen. This approach
452 worked well for Kevlar and other polymer fibres, but carbon and glass fibres broke too easily under
453 rotation. Using this method, the smallest inter-fibre distance achievable was four times the fibre diameter.
454 This has been considered by Li *et al.* [10] to be insufficiently close to study meaningful stress transfer;
455 however, elsewhere, a much higher ratio of 15 fibre diameters has been advanced as a reasonable stress
456 transfer radius, (Cox model [52]). Jones and DiBenedetto [53] modified this approach by using rotating
457 brass combs with spacings of 101 μm. Interfibre spacing was controlled by adjusting the angle of rotation
458 on the device, before depositing the aligned dry fibres in a silicone mould for curing. Li, Grubb and Phoenix
459 [10] reported yet another fibre-spacing apparatus, which used spacers to maintain fixed, known fibre
460 spacings. A schematic of the MFFT apparatus is shown in Figs. 2 and 3 of Li *et al.* [10] and is similar to the
461 apparatus shown in Figure 6. This was used to perform MFFT on an epoxy-based composite with Nicalon
462 silicon carbide fibres of 15 μm diameter. Fibres were stabilized in a group of three on a frame by tensing
463 each fibre with freely-hanging glass rods on both sides as weights (1 g). The fibres were maintained at
464 regular inter-fibre spacings along the top of the frame. Then the silicone mould was raised underneath the
465 fibre assembly on an independent stage until the fibres were aligned correctly within the appropriate
466 cavities, without touching the mould walls. The epoxy mixture was then injected into the cavities from
467 either end using pipettes in such a way as not to unduly disturb the fibres. Once the moulds were filled, the
468 epoxy mixture was cured as described above. Finished specimens had a typical thickness of 1 mm, and were
469 polished after curing to eliminate rough edges, which could cause premature fracture and bias desired
470 results.

471 The epoxy was a mixture with 70:30 mass ratio of DER 331 (diglycidyl epoxide of bisphenol A) to DER 732
472 (polyglycol diepoxide). It was cured with DEH 26, a tetraethylene pentamine. Specimens were cured at
473 room temperature for 24 h and for 3 h at 80 °C in silicone rubber moulds. Importantly, the fracture strain
474 of the epoxy resin was much higher; 12.2 %, compared with that of the fibre; 1.6 %.

Typically, the fragmentation tests were executed with a gauge length of 20 mm on an Instron Tensile Tester Model 1122 at a strain rate of 0.0025 min^{-1}. Some tests were monitored *in-situ*, albeit somewhat remotely, using a telescope (Questar Model QM1) with 100x magnification and focal length of 1 m. Teflon was mounted behind the specimen to enhance the contrast of the embedded fibres in images, which were displayed on a local TV screen. The Nicalon fragmentation was typically complete at a strain of 5 %. Fragment lengths were measured after test completion using an optical microscope with a grid-calibrated eye-piece. Micrographs of some specimens were also taken on separate strain rigs implementing equivalent strains to the Instron, in order to study photoelastic, birefringence patterns (Olympus Model PME).

Holmes et al. [54] designed a substantially different system to those used by Phoenix and others previously. Here, an integrated testing system was designed where interval-censored photographs of fibre-bundles could be recorded in tandem with the recording of load data *in-situ* during a uni-directional tensile test of a dogbone specimen.

Overall, while MFFT test equipment has achieved increasingly more precise control over fibre uniaxial testing, the management of fibre tension during fibre embedding can be difficult due to the absence of an effective means of filament local tension measurement. The embedment process is also typically manual which introduces variability in initial fibre tension and potential undetected crazes on fibre surfaces that can precipitate premature failure. The stress relaxation state of individual fibres in an array is also not fully accounted for in published methods (which also indicates the need for in-situ tension measurement during embedment). Nevertheless, advances in microactuators, sensors and programming indicate that all of these challenges can be addressed.

3.2 MFFT Literature Data

A number of workers have reported important data for MFFT, albeit using equipment which has tended to diverge greatly in design, and also using different composite systems, testing techniques and protocols. Therefore, it is not always possible to make direct comparisons between their respective reports, or draw general conclusions about physical phenomena occurring in embedded fibre arrays generally. However, some fundamental observations have been made by some of these authors, which in some cases directly contradict response predicted by the shear-lag family of models based on the analysis of Cox.

Jones and DiBenedetto, [53], performed a MFFT using their rotating brass 'comb' system to mount precisely co-aligned fibres in a silicone mould prior to filling resin. They performed same-fibre MFFT and hybrid or

different-fibre MFFT tests. These featured two coated E-glass fibres (A-1110 and A-163), AS4 and IM6-G carbon fibres, and Kevlar 49. The combinations were 1) AS4/IMG6-G, 2) A-1110, Eglass/A163 Eglass, 3) Kevlar 49/AS4 carbon fibre, and 4) A-1110 Eglass/AS4 carbon. For the AS4 test, nine fibres were aligned with interfibre spacing of approximately 14 fibre diameters. It was found that the mean fragment length of two such samples was almost equivalent to that measured for the equivalent AS4 SFFT test (0.69 mm, MFFT, 0.72 mm SFFT), although the fibre fragment length distribution for MFFT was somewhat broader. This may have been due to an incidentally weak SFFT fibre interface compared with that of the MFFT fibres, which may have resulted in a longer stress transfer length. Additionally, where there was inter-fibre separation of seven or more fibre diameters, random fracture was observed. However, for inter-fibre spacings smaller than seven diameters, evidence of co-ordination between fracture locations of adjacent fibres was observed. Co-ordinated fractures between adjacent fibres were attributed to stress concentrations at the intact fibre caused by stress relinquished by the broken neighbouring fibre. The authors failed to determine fractures with sufficient certainty in the Kevlar 49 fibres, but stated that the Kevlar 49 fibre failed in shear based on micrographs and consistent with the observations of Wagner and Steenbakkers. This fibre shearing had the effect of lessening the concentration of stress concentrations in the neighbouring intact fibres. By contrast, the two coated glass fibres showed clearly co-ordinated fractures between fibres in each case, even at six fibre diameters' displacement, which to that point had been believed to be the outer limit of significant stress transfer between two fibres. As seen for the AS4 fibres, there was little significant difference between average critical fragment length under the SFFT and MFFT (0.77 mm, MFFT v. 0.78 mm, SFFT), although the fibre fragment length distribution for MFFT was broader. However, the MFFT/SFFT distinction was significant for the methyl silane-coated E-glass fibres. Here, the critical length of the SFFT was 0.95 mm, compared with the MFFT value of 1.28 mm. The longer MFFT length was thought to be caused by more severe debonding and interface failure caused by stress concentrations induced by fracturing neighbouring fibres. (A-163 was a poor sizing agent, inducing a weak interface). The hybrid MFFT tests delivered further insights, albeit the systems being studied were highly artificial and the results would be unlikely to apply to a commercial system. For AS4/IM6-G, the two fibres fractured in a highly co-ordinated manner with nearly equivalent critical fibre fragment lengths. However, the common hybrid critical length (0.81 mm) of each fibre was higher both than that of the AS4 fibre alone (0.72 mm), and the IM6-G fibre alone (0.57 mm). The A1110/A-163 E-glass hybrid system (alternating in each type) showed high co-ordination of fractures between fibres, with both fibres showing slightly lower

critical fibre fragment length (A-1110 = 0.71 mm compared with an SFFT value of 0.78 mm; A-163 = 0.85 mm compared with SFFT 0.95 mm) This was the opposite trend to that observed for the AS4/IM6-G system showing that differences between both test modes were primarily due to differences in the interface quality of the constituent fibres rather than being determined solely by the test mode or inter-fibre separation. In particular, for this system, the authors observed that a crack occurring at the A-1110 fibre was arrested at the poorly sized A-163 fibre since the weaker interface directed the energy along the interface via debonding, rather than permitting a further fibre fracture allowing the crack to propagate along the entire section of the composite. Thus, in this context, a relatively weak interface could be beneficial in arresting fibre breakage, an observation more easily facilitated by this type of MFFT where one plane of fibres could be studied and fibre volume fraction, interfibre spacings and fibre coatings could be closely controlled. The authors also performed computer modeling of the process using a technique by DiLandro et al. [55] based on a local load sharing (LLS) model where stress concentration at an incipient fracture site on an intact fibre were calculated based on a knowledge of the number of surrounding fracture sites, and the type of neighbouring fibres. The computer model established that fibres in the hybrid 1000-fibre MFFT systems experienced significantly lower transferred stress from a neighbouring fracture than the equivalent control fibre (SFFT). For high-extension glass fibres placed adjacent to low extension carbon fibres, this resulted in less fracture of the latter, resulting in higher measured mean strength of the carbon fibres. Increases in carbon fibre strength in these situations varied dramatically: from 24% for 'tightly packed' fibres to as much as 97% for more 'dispersed' fibres.

Grubb, Phoenix et al. [9] reported MFFT data for three, five or seven Nicalon fibres spaced regularly on a frame as discussed above, where fibres were typically separated by one fibre diameter. They concluded that the mean fibre fragment length was a function both of inter-fibre separation and the number of fibres present in the parallel fibre array. Specifically, mean fragment length increased where inter-fibre distance was smaller, and also when more fibres were present in the system. Generally, longer mean fragment length (hence fewer fragments per unit length fibre) indicates that the fibre is absorbing less stress from the matrix, when surrounded by other fibres at sufficient proximity, because they are also absorbing stress. Longer mean fragment length can also indicate lower stress transfer efficiency of the interface or a lower interfacial shear strength, since if either of the latter are low, the interface may fail before it can transfer sufficient stress to the fibre to enable fragmentation.

However, this increase of mean fragment length in the presence of closer fibres directly contradicted the predictions of the Cox model, where *a decrease* in mean fragment length was expected as the matrix radius r_m decreased. More fundamentally, if critical fibre fragment length is calculated as a direct function of mean fibre fragment length, this means that *derived values of critical fibre fragment length, and hence, IFSSh (calculated via Eqn. 2 (Kelly Tyson, [8,56]), are very dependent on experimental conditions rather than being independent material properties of the interface itself as they should be by definition.* This deficiency is most readily seen in tests involving multiple fibres aligned closely in parallel, and is evident throughout the MFFT literature. Grubb et al. [9] suggested that the shear-lag models, which had been designed to model the behaviour of single fibre fragmentation in a direction along the longitudinal fibre axis, were intrinsically incapable of modeling stress transfer *between* fibres. Despite the presence of an r_m parameter in the Cox-type models, which emerged mathematically in their development, there was no constitutive physical model for stress transfer to make r_m representative of real systems. Consequently, Grubb et al. [9] advanced a number of literature models, in addition to their own, which were intended to more closely model such fibre-fibre interactions, and contained an interaction radius parameter similar to r_m. These two geometrically-constructed fibre sector angle and overlap area models were claimed to deliver better agreement with their experimental Raman data than either the local load sharing (LLS) or Eitan & Wagner models, based on a comparison of Raman-derived and calculated values of stress concentration factor, K_c, for each binary fibre combination. However, despite the relative accuracy of these models, they are based exclusively on geometric considerations, i.e., they calculate either a 'line of action' or 'area of action' between two fibres and assume that stress transfer will be proportional to either of these factors. There is no provision for including factors such as viscoelasticity of the matrix, the associated time-delay of force transfer because of force amplitude damping effects or other factors. Nevertheless, they provide a useful conceptual framework, with which to build an effective comprehensive constitutive model of stress transfer through a matrix.

3.3 Areas for Improvements in MFFT

MFFT tests require improvements in the following areas as follows:

1. MFFT equipment has tended to diverge greatly in design, and also using different composite systems, testing techniques and protocols. Therefore, it is not always possible to make direct comparisons between their respective reports, or draw general conclusions about physical phenomena occurring in embedded fibre arrays generally. Thus, equipment needs to be improved and standardised.
2. Existing models for stress transfer between fibres during the fragmentation process rely on geometrical models for stress transfer that project stress transfer between fibres as a sole function of area-of-sight, or in limiting cases as decaying functions of inter-fibre separation. These models are currently insufficient for modelling stress transfer as a function of matrix properties, especially considering the wide window of properties for existing commercial resin systems. Constitutive matrix stress transfer models are needed.
3. Current MFFT models do not incorporate terms to calculate matrix vibration as a function of fibre fracture shock. The effect of shock is also a sensitive function of matrix viscoelasticity, so that a comprehensive model for MFFT will need to incorporate terms for the transfer of energy between fibres by acoustic shock.

4.0 Measurements of Fibre Matrix Interfaces under other loading conditions

To now, this review has focused almost exclusively on techniques used to interrogate fibre-matrix interfaces under uniaxial tension. However significant work has also been done on composites under fibre-axis compression, tensile-compressive cyclic loading and on commercial composites. For composite systems tested under compression, Goutianos et al. [57, 58] published two studies examining fibre matrix stress transfer for carbon epoxy composites under uniaxial compression along the fibre axis. Both studies examined interface stress transfer efficiency under both compression and tension, with tension loading being used as a control case. In [57], they established that the maximum interfacial shear stress measured was a function of applied strain, but, surprisingly, it was independent of the type of loading, i.e., (whether compressive or tensile). This finding is consistent with the idea that the maximum interfacial shear stress should represent the intrinsic interfacial shear strength of the interface, a material property, which should indeed be independent of the direction of uniaxial loading. However other differences were observed, i.e., the authors observed much lower stress

transfer lengths in fibre fragments under compression than those under tension (40-80 μm v. 450-500 μm). This was accounted to the fact that when compressed fibres fragmented, they were still able to transmit stress through the break via mutual compression of adjacent fragments, a mechanism obviously not available during uniaxial tension. Additionally, it was found that the distribution of fibre breaks in a compressed system was far more uniform with a more reproducible mean fragment length than that determined for fibre systems under uniaxial tension. This was explained by the fact that tensile failure in a fibre is governed by the more random distribution of crazes and flaws that determine the location and order of fibre fragmentation, whereas compression failure is driven by failure phenomena at the microcrystalline level of the carbon fibres. Finally, Koimtzoglou et al. [59] extended work in this direction by examining cyclic loading at maximum 0.5% strain of one M40-40B Toray fibre in an Epikote 828 epoxy resin under uniaxial tension/compression to determine the fatigue properties of the fibre-matrix interface. They reported the progress of fibre fragmentation during a 2 Hz test over a 2 mm fibre length as follows: 1 fragment at 1 cycle; three fragments at 10,000 cycles; four fragments at 500,000 cycles and five fragments at 1,000,000 cycles, representing a final break density of 2.5 mm^{-1}. Raman spectroscopy showed that there was a residual stress of ca. 400 MPa in the vicinity of the first break, with a stress development length of ca. 600 μm to a stress plateau of 4.4 GPa at a fibre strain of 1.0%. At 1000 cycles, the first plateau showed a stress increase to 4.8 GPa, while the second showed one of 4.0 GPa at an applied fibre strain of 1.2%. Near-stress-saturated fragments were then observed at 100,000 cycles, which showed triangular stress distributions peaking at between 2.4 and 2.8 GPa at a fibre strain of 0.6%. The maximum IFSS calculated at 1 cycle was between 45 and 50 MPa, values which ultimately remained stable for practically all fragments formed at the end of the test (1,000,000 cycles). Again, this result demonstrated that calculated IFSSh was largely independent of fatigue stage, which is consistent with its definition as a material property of the interface. However, the work in [57-59] concerned single fibres rather than parallel arrays. It is clear that more work remains to be done in this area to interrogate compression and fatigue effects in multi-fibre arrays, and the formal fibre break statistics observed during compression also requires further characterisation.

5.0 Discussion

In this paper, the history and current state of the fibre fragmentation technique (augmented with Raman spectroscopy) have been described for the determination of interfacial shear strength in fibre-reinforced composite systems.

However, none of the fragmentation techniques described have yet achieved sufficient reliability to form the basis of a universal standard for the measurement of absolute interfacial shear strength that could be used to estimate laminate ILSS. The reasons for this are many: 1) These indirect techniques do not result in a direct measurement of interfacial shear strength but rely on non-optimal equations to calculate IFSS as a derived quantity from first-order load-deflection curves and/or fibre fragmentation statistics coupled with load-time data, 2) Non-fibre-contact 'embedded fibre' techniques such as fibre fragmentation are currently time-consuming and non-trivial to perform, featuring complex model specimen preparation and complex loading conditions not fully understood at the interface level via existing models (e.g. Kelly-Tyson, shear-lag). 3) Direct-fibre-contact techniques, though simple to execute, do not properly capture interface behaviour that actually applies to fibres fully embedded in resins. 4) The matrix strain-to-failure commonly required to execute fragmentation tests are usually far higher than that which would apply in 'real' composite structures 5) Recent findings by McCarthy et al. [60] of Uniform fragmentation break statistics that apply to the fragmentation test imply no deterministic mechanism for formation of fibre breaks during SFFT or MFFT. This appears to defy the classical assumption of stress development over fibre fragments made by shear lag and Kelly-Tyson models. This renders it difficult to calculate IFSSh from these tests without the improvisation of a radically different theoretical framework to describe stress transfer and fibre fragmentation from first principles. Specifically, the concept of a 100%-ineffective stress transfer length is seriously challenged by these statistical findings, which implies that at the very most there is reduced probability of fragmentation along these lengths rather than a complete impossibility of a break forming.

More fundamentally than this, it is clear that interfacial shear strength values derived from fibre fragmentation statistics are dependent on test parameters such as inter-fibre separation distance (in MFFT*) that should have no effect on what should be an intrinsic property of the particular chemistry of the fibre-matrix interface alone*. This presents the scenario that one can devise a fragmentation test at high volume fraction that closely models the behavior of a real composite, but is incapable of isolating the actual

673 intrinsic shear strength of the interface. Alternatively, one can pursue a SFFT that provides a closer estimate
674 of IFSSh but does not capture stress concentration effects introduced by nearest neighbour fibres as is
675 possible via the MFFT. Finding a technique that achieves a compromise between these two extreme cases
676 remains the challenge at time of writing.

677 Apart from determination of IFSSh, which is a mechanical property of the fibre-matrix interface, there are
678 also techniques that measure surface energy and chemical energy of the fibre coatings/sizings. These
679 include contact angle measurements, [61] inverse gas chromatography, [62] and precise atomic force
680 microscopy, [63]. However, at present, there is no robust model that can predict interfacial shear strength
681 on the basis of the known chemical bond or surface energy of an interface. Were this to be developed, it
682 would arguably be much easier to customize interface chemistry to balance desired strength, toughness
683 and shear strain-to-failure.

684 The original Griffith expression which includes a term for surface energy, γ, might provide a precedent for
685 how such a relationship could be conceived and validated, i.e., Eqn 19, [64].

686 $$\sigma_f \sqrt{a} = \sqrt{\left({}^{2E\gamma}/_{\pi}\right)} \tag{19}$$

687 Here σ_f is the fibre tensile stress, a is the crack length, and E is the material modulus. However, the surface
688 energy referred to by Griffiths does not capture the covalent or hydrogen bonding energy of the interface
689 chemistry that would be distinctive for various common fibre sizings. The surface energy effectively
690 expresses physical attractive/repulsive forces at the interface that are not necessarily equivalent to energy
691 of chemical debonding at the interface, but may be related.

692 At present, optimization of interface chemistry is done in an iterative manner by depositing a fibre sizing
693 formulation and performing tests at a macroscopic level, e.g., using lap-shear testing to assess bond
694 strength. However, no constitutive relation has been proposed between chemical and mechanical
695 properties (apart from the Griffith relation above) that would allow mechanical properties to be
696 customized in a controlled, precise and predictable manner by molecular design.

697 Lastly, qualitative detection methods for interface bonding conditions are in their infancy. Recent work by
698 Zammarano et al. [65] showed that Forster Resonance Energy Transfer (FRET) could be used to identify
699 the interface using optical microscopy to make a qualitative evaluation of the size and condition of a
700 polymer composite interface, a potentially revolutionary technique for revealing the interface by

conventional confocal microscopy accessible to many laboratories. However, this technique is hampered by a number of challenges: a) a system with an embedded interface can only be studied if the matrix is significantly transparent, b) there must be robust and complete coverage of both interfaces by the relevant donor and acceptor dyes to eliminate the possibility of false positive indications of interface rupture.

Thus, both detection methods and mechanical tests for interface strength and quality are significantly underdeveloped in various ways. This presents a significant challenge to the engineering design community in understanding the link between adhesive and sizing chemistries and mechanical/degradative performance. Arguably, there is a significant case for dedicating increased resources and attention to the solution of the scientific and technological challenges necessary to produce standardized descriptive models and measurement standards for the interface. If this is achieved, it is highly likely that it would enable radically improved control of interface properties by a more precisely customised chemistry of sizings. After fifty years of activity in mechanical characterization of the fibre matrix interface, it is perhaps time to consolidate numerous approaches into one, unified comprehensive model of the fibre matrix interface and fibre-fibre stress transfer that explains macroscopic behavior of composites. The critical fibre fragment length has an impact on composite fracture toughness and affects the notched strength and hence notch sensitivity of the composite system [66], so its accurate evaluation becomes important in design. It has been seen earlier that it also relates to the IFSS that may influence the initiation of matrix cracking in a cross ply or multidirectional laminate [67, 68] which in turn would trigger delaminations at different ply interfaces [69, 70] that could lead to fibre breakage or fibre instabilities when loaded in compression [71, 72] and ultimately to catastrophic failure. Currently, uncertainties in the value of the IFSSh and ILSS lead to unnecessarily high load safety factors and overweight structural configurations, reducing the benefit offered by fibre reinforced polymer composites [73].

References

1 Thomason JL, Yang L. Interface strength in glass fibre–polypropylene measured using the fibre pull-out and microbond methods. Compos. Part A, 2010; 41:1077–1083.

2 Hutchinson JW, Jensen HM. Models of fiber debonding and pullout in brittle composites with friction. Mech Mater, 1990; 9: 139–163.

3 Chen Z, Yan W, A shear-lag model with a cohesive fibre–matrix interface for analysis of fibre pull-out. Mech. Mater., 2015; 91: 119–135.

4 Kalinka G, Leistner A, and Hampe A, Characterisation of the fibre/matrix interface in reinforced polymers by the push-in technique. Compos. Sci. Technol. 1997; 57: 845–851.

5 Rodriguez M, Molina-Aldareguia JM, Gonzalez C, Llorca J. A methodology to measure the interface shear strength by means of the fiber push-in test. Compos. Sci. Technol. 2012; 72: 1924–32.

6 Jager J, Sause MGR, Burkert F, Moosburger-Will J, Greisel M, and Horn S. Influence of plastic deformation on single-fibre push-out tests of carbon fiber reinforced epoxy resin. Compos. Part A, 2015; 71: 157–167.

7 Cox HL, The elasticity and strength of paper and other fibrous materials. Br. J. Appl. Phys., 1952;3:72-78.

8 Kelly A, Tyson WR, Zackay VF, in *High Strength Materials*, New York: John Wiley & Sons, 1964, p. Chapter 13, 578.

9 Grubb DT, Li ZF, and Phoenix SL, Measurement of Stress Concentration in a Fiber Adjacent to a Fiber Break in a Model Composite, Compos. Sci. Technol., 1995; 54: 237–249.

10 Li ZF, Grubb DT, Phoenix SL, Fiber Interactions in the Multi-fiber Composite Fragmentation Test, Compos. Sci. Technol., 1995; 54: 251–266.

11. Galiotis C, Young RJ, Batchelder DN. A Resonance Raman Spectroscopic Study of the Strength of the Bonding Between an Epoxy Resin and a Polydiacetylene Fibre. J Mater Sci Lett. 1983; 2(6):263-266.

12. Tuinstra F, Koenig JL. Raman spectrum of graphite, J Chem Phys. 1970;53(3):1126-1130.

13. Tuinstra F, Koenig JL. Characterization of graphite fiber surfaces with Raman spectroscopy. J Compos Mater. 1970;4(4):492–499.

14. Mitra VK, Risen WM, Baughman RH. A laser Raman study of the stress dependence of vibrational frequencies of a mono-crystalline polydiacetylene. J Chem Phys. 1977; 66(6):2731–2736.

754 15. Penn L, Milanovich F. Raman spectroscopy of Kevlar 49 fibre. Polymer. 1979;20:31-36.
755 16. Galiotis C, Young RJ, Yeung PHJ, Batchelder DN. High Modulus Polydiacetylene Single Crystal
756 Fibres. J Mater Sci. 1984;19:3640-3648.
757 17. Galiotis C, Young RJ, Batchelder DN. Solid-State Polymerisation and Physical Properties of
758 Bis(ethyl urethane) of 2,4-hexadiyne-1,6-diol, Part II: Resonant Raman Spectroscopy. J Polym Sci
759 Part B-Polym Phys. 1983;21:2483-2494.
760 18. Robinson IM, Zakikhani M, Day RJ, Young RJ, Galiotis C. Strain dependence of the Raman
761 frequencies for different types of carbon fibres. J Mater Sci Lett. 1987;6:1212-1214.
762 19. Galiotis C, Batchelder DN. Strain Dependences of the First and Second Order Raman Spectra of
763 Carbon Fibres. J Mater Sci Lett. 1988;7:545-547.
764 20. Guild FJ, Vlattas C, Galiotis C. Modelling of stress transfer in fibre composites. Compos Sci
765 Technol. 1994;50:319.
766 21. Schadler LS, Galiotis C. Fundamentals and applications of micro Raman spectroscopy to strain
767 measurements in fibre reinforced composites. Int Mater Rev. 1995;40(3):116.
768 22. Melanitis N, Galiotis C, Tetlow PL, Davies CKL. Interfacial Shear Stress Distribution in Model
769 Composites; Part 2, Fragmentation studies on Carbon Fibre/ Epoxy systems. J Compos Mater.
770 1992; 26:574-610.
771 23 Melanitis N, Galiotis C, Interfacial micromechanics in model composites using laser Raman
772 spectroscopy, Proc Roy. Soc. Lond. A. 1993;440:379-398.
773 24. Melanitis N, Galiotis C, Tetlow PL, Davies CKL. Monitoring the micromechanics of reinforcement
774 in carbon fibre/epoxy resin systems. J Mater Sci. 1993; 28:1648–54.
775 25. Galiotis C. Interfacial Studies on Model Composites Using Laser Raman Spectroscopy. Compos Sci
776 Technol. 1991;42:125.
777 26. Jahankhani H, Galiotis C. Interfacial shear stress distribution in model composites (Part. 1). J
778 Compos Mater. 1991;25: 609-631.
779 27. Eichhorn SJ, Young RJ, Jin SY. Controlling and mapping interfacial stress transfer in fragmented
780 hybrid carbon fibre-carbon nanotube composites. Compos Sci Technol. 2014; 95: 114-120.
781 28. Galiotis C. Paipetis A, Marston C. Unification of fibre/matrix interfacial measurements with
782 Raman microscopy, J. Raman Spectrosc. 1999; 30, 899–912.

29. Frank O, Tsoukleri G, Riaz I, Papagelis K, Parthenios J, Ferrari AC, Geim AK, Novoselov KS, Galiotis C. Development of a universal stress sensor for graphene and carbon fibres. Nature Comms, 2011;2(255):1.

30. Anagnostopoulos G, Parthenios J, Galiotis C. Phonon stress sensitivity for interface characterization of fibrous composites at various temperatures, Acta Materialia, 2007;55(11):3783-3793.

31. McCartney LN. New theoretical model of stress transfer between fiber and matrix in a uniaxially fibre-reinforced composite. In: Proc R Soc Lond. 1989. A425 p. 215-244.

32. Whitney JM, Drzal LT. Axisymmetric stress distribution around an isolated fibre fragment. In: ed. Johnston NJ, Toughened Composites. Philadelphia, PA: ASTM; 1987. p. 179-196.

33. Jin S-Y, Youn RJ,Eichorn SJ. Controlling and mapping interfacial stress transfer in fragmented hybrid carbon fibre–carbon nanotube composites. Comp Sci Tech 2014;100:121-127.

34. Nairn JA. On the use of shear-lag methods for analysis of stress transfer unidirectional composites. Mech Mater. 1997;26:63-80.

35. Drzal LT, Rich MJ, Camping JD, Park WJ. In: Proceedings of the 35th Annual Technical Conference. Reinforced Plastics/Composites Institute and The Society of the Plastics Industry, Inc.; p. 1.

36. Harlow DG, Phoenix SL. The chain-of-bundles probability model for the strength of fibrous materials I: Analysis and conjectures. J Comp Mat. 1978;12:195–214.

37. Harlow DG, Phoenix SL. The chain-of-bundles probability model for the strength of fibrous materials II: A numerical study of convergence. J Comp Mat. 1978;12:314–34.

38. Wagner HD, Eitan A. Interpretation of fragmentation phenomenon in single-filament composite experiments. Appl Phys Lett. 1990;56:1965-1967.

39. Chawla KK. Composite Materials Science and Engineering. New York: Springer; 1998.

40. James MN. Failure as a Design Criterion [Internet]. 2003. Available from: http://www.tech.plym.ac.uk/sme/FailureCases/Failure.htm

41. Agarwal BD, Broutman LJ. Analysis and Failure of Fiber Composites. New York: John Wiley & Sons; 1990. p. 87.

42. DiBenedetto AT. Measurement of the thermomechanical stability of interphases by the embedded single fiber test. Compos Sci Technol. 1991;42:103-123.

43. Drzal LT, Dusek K. In: Epoxy Resins and Composites II. New York: Springer Verlag; 1986. p. 1.

44. Holister GS, Thomas C. Fibre Reinforced Materials. London: Elsevier Publishing Co. Ltd.; 1966.

45. Rosen BW. Tensile failure of fibrous composites. AIAA J. 1964;1985-1991.

46. Wadsworth NJ, Spilling I. Load Transfer from Broken Fibres in Composite Materials. Br J Appl Phys J Phys D. 1968;1:1049-1058.

47. Drzal LT, Madhukar M. Fibre-matrix adhesion and its relationship to composite mechanical properties. J Mater Sci. 1993;28:569–610.

48. Steenbakkers LW, Wagner HD. Technical Report. The Weizmann Institute of Science: Polymeric Composites Laboratory; 1988. Report No.: PCL-88-02.

49 Gulino R, Phoenix SL. Weibull strength statistics for graphite fibres measured from the break progression in a model graphite/glass/epoxy microcomposite. J Mater Sci. 1991;26:3107–18.

50. Gulino R, Schwartz P, Phoenix SL. Experiments on shear deformation, debonding, and local load transfer in a model graphite/glass/epoxy microcomposite. J Mater Sci. 1991;26:6655–72.

51. Wagner HD, Steenbakkers LW. MIcrodamage analysis of fibrous composite monolayers under tensile stress. J Mater Sci. 1989;24:3956–75.

52. Cox HL. The elasticity and strength of paper and other fibrous materials. Br J Appl Phys. 1952;3:72-79.

53. Jones KD, Dibenedetto AT. Fiber fracture in hybrid composite system. Compos Sci Technol. 1994;51:53-62.

54. Holmes GA, Wesson S, McDonough WG, Kim JH, Netravali AN, Walker JN, et al. An automated testing machine for monitoring the evolution of fiber breaks. J Mater Sci. 2009;44:2007-2015.

55 DiLandro L, Dibenedetto AT, Groeger. The effect of fiber–matrix stress transfer on the strength of fiber–reinforced composite materials. J Polym Compos. 1988;9:209-221.

56. Kelly A, Tyson WR, Zackay VF. Fiber Strengthened Materials. In: High Strength Materials. New York: John Wiley & Sons; 1964. Chapter 13, p. 578-583.

57. Goutianos S., Peijs T, Galiotis C. Mechanisms of stress transfer and interface integrity in carbon/epoxy composites under compression loading. Part I. Int. J. Solids & Structures, 3217-3231: 39(12), 2002.

58. Goutianos S, Peijs T, Galiotis C, Comparative Assessment of Stress Transfer Efficiency in Tension and Compression. Composites Part A, 2002; 33:1303-1309.

59. Koimtzoglou C, Kostopoulos V, Galiotis C, Micromechanics of Reinforcement and Damage Initiation in Carbon Fibre/Epoxy Composites under Fatigue Loading. Composites Part A, 2001; 32: 457-471.
60. McCarthy ED, Kim JH, Heckert NA, Leigh SD, Gilman JW, Holmes GA, The fiber break evolution process in a 2-D epoxy/glass multi-fiber array. Comp Sci Tech. 2015;121;73-81.
61. Yuan Y, Randall Lee T. Chapter 1. Contact Angle and Wetting Properties. In: Bracco G, Holst B, editors. Surface Science Techniques. Berlin & Heidelberg: Springer Verlag; 2013. (Springer Series in Surface Sciences).
62. Mohammadi-Jam S, Waters KE. Inverse gas chromatography applications: A review. Adv Colloid Interface Sci. 2014;212:21–44.
63. Neuman KC, Nagy A. Single-molecule force spectroscopy: optical tweezers, magnetic tweezers and atomic force microscopy. Nat Methods. 2008;5(6):491–505.
64. Griffith AA. In: Philosophical Transactions of the Royal Society of London, Series A. 1920. p. 163–98.
65. Zammarano M, Maupin PH, Sung L, Gilman JW, McCarthy E., Kim YS, et al. Revealing the interface in polymer nanocomposites. ACS Nano. 2011 Aug 4;5(4):3391–9.
66. Hitchen SA, Olgin SL, Smith PA. The effect of fibre length on fracture toughness and notched strength of short carbon fibre/epoxy composites. Composites. 1994;25(6):407–13.
67. Katerelos DTG, Kashtalyan M, Soutis C. Matrix cracking in polymeric composites laminates: Modelling and experiments. Compos Sci Technol. 2008;68(12):2310–2317.
68. Kashtalyan M, Soutis C. Stiffness and fracture analysis of laminated composites with off-axis ply cracking. Compos Part -Appl Sci Manuf. 2007;38(4):1262–1269.
69. Kashtalyan M, Soutis C. The effect of delaminations induced by transverse cracks and splits on stiffness properties of composite laminates. Appl Sci Manuf. 2000;31(2):107–119.
70. Kashtalyan M, Soutis C. A study of matrix crack tip delaminations and their influence on composite laminate stiffness. Adv Compos Lett. 1999;8(4):149–155.
71. Soutis C, Guz IA. Fracture of layered composites by internal fibre instability: effect of interfacial adhesion. Aeronaut J. 2006;110(1105):185–190.
72. Soutis C, Turkmen D. Influence of shear properties and fibre imperfections on the compressive behaviour of GFRP laminates. Appl Compos Mater. 1996;2(6):327–342.

872 73. Soutis C. Fibre reinforced composites in aircraft construction. Prog Aerosp Sci. 2005;41(2):143–
873 151.
874

Figures

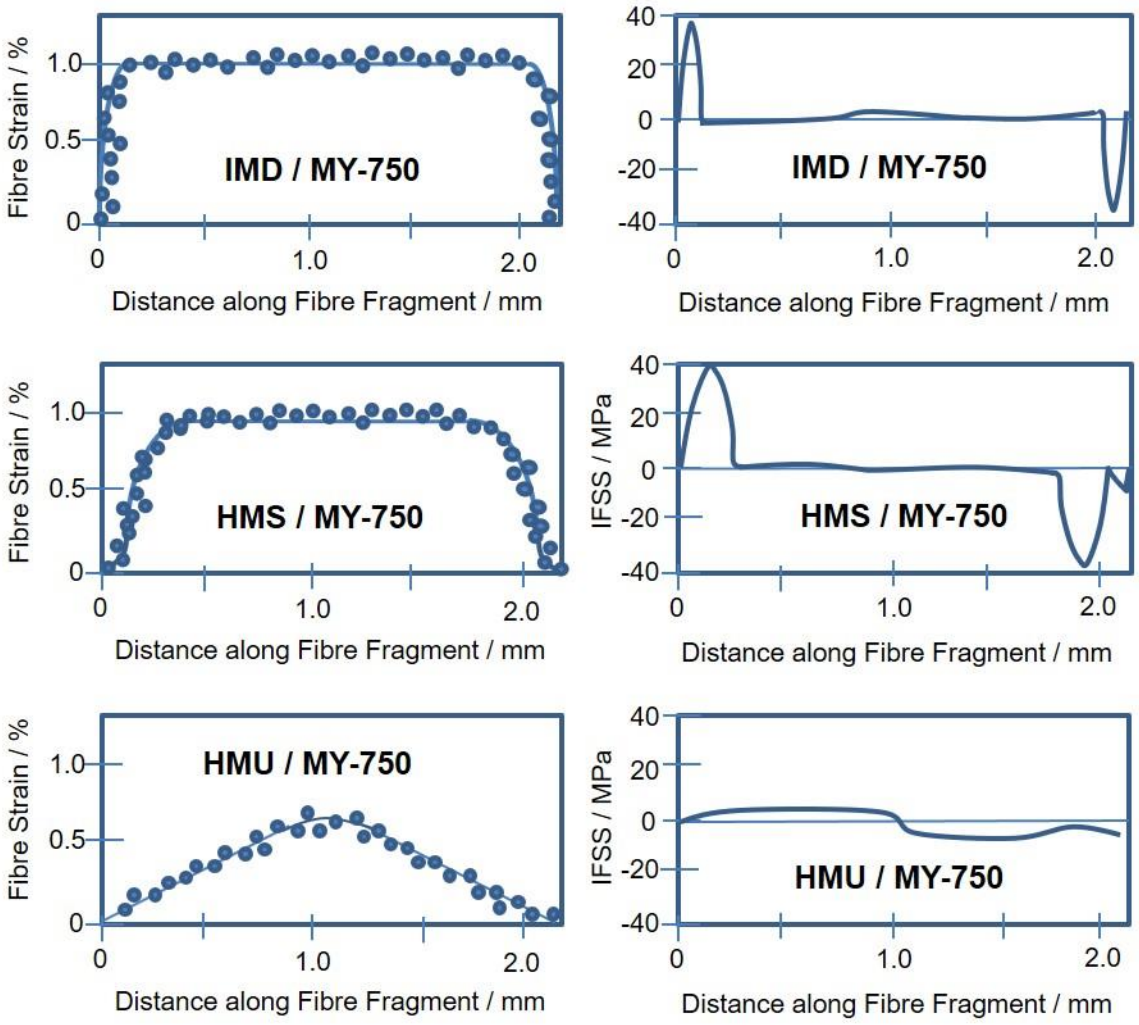

Figure 1. Measured Strain Profile and Derived IFSS Profile for three fibre-epoxy systems at an applied strain of 1%, Based on Schadler et al. [21].

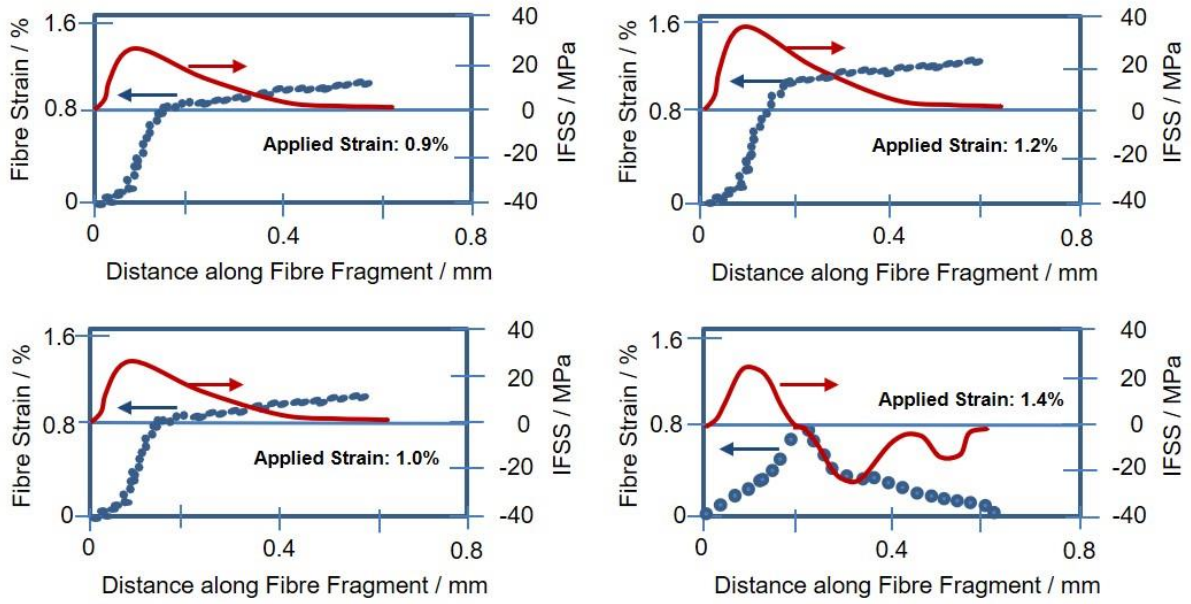

880

881 **Figure 2. Measured Strain Profile and Derived IFSS Profile, Based on Melanitis et al. [22].**

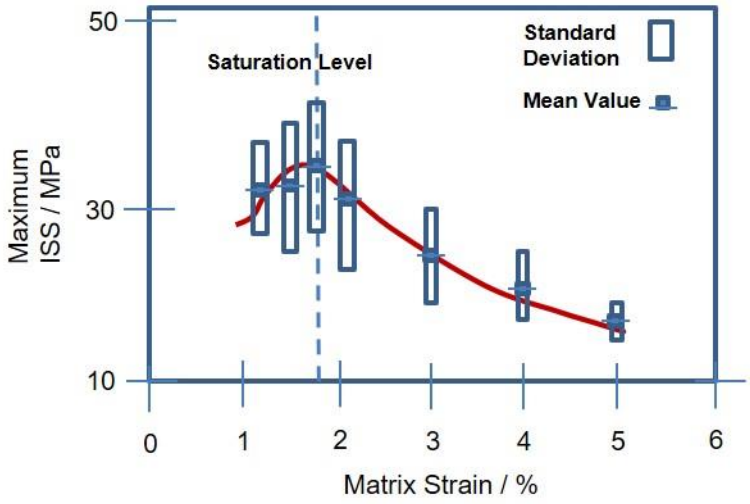

882

883 **Figure 3. ISS Maxima plotted at different axial specimen strain levels (different fragmentation**

884 **experiments), Based on Melanitis et al., [22].**

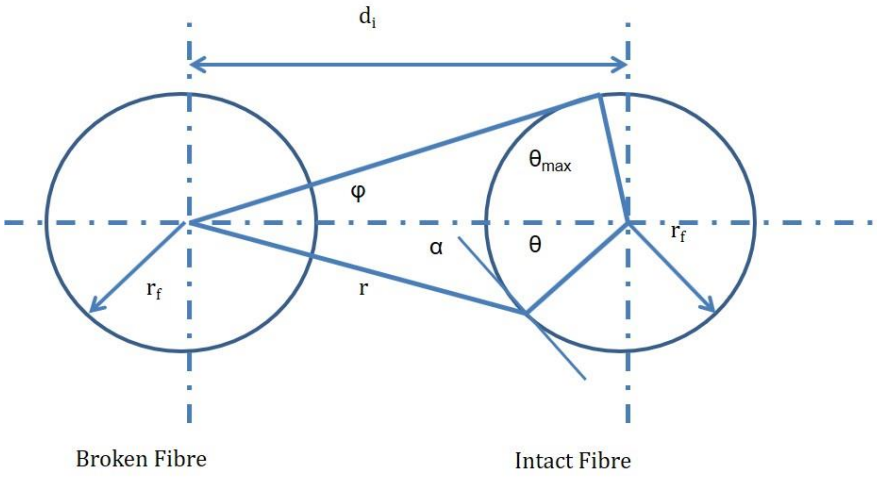

885

886 **Figure 4. Geometry of Interfibre stress transfer model of Eitan and Wagner, Based on [38].**

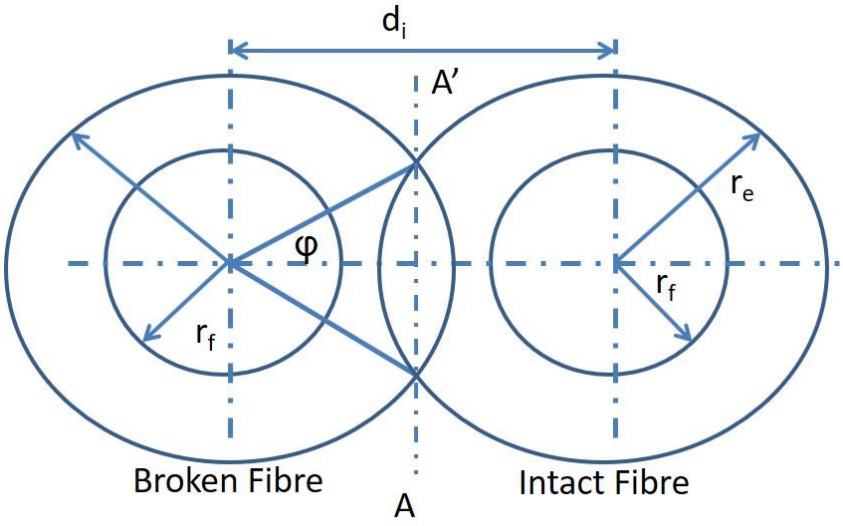

887

888 **Figure 5. Geometry of Interfibre stress transfer model of Grubb et al., Based on [9].**

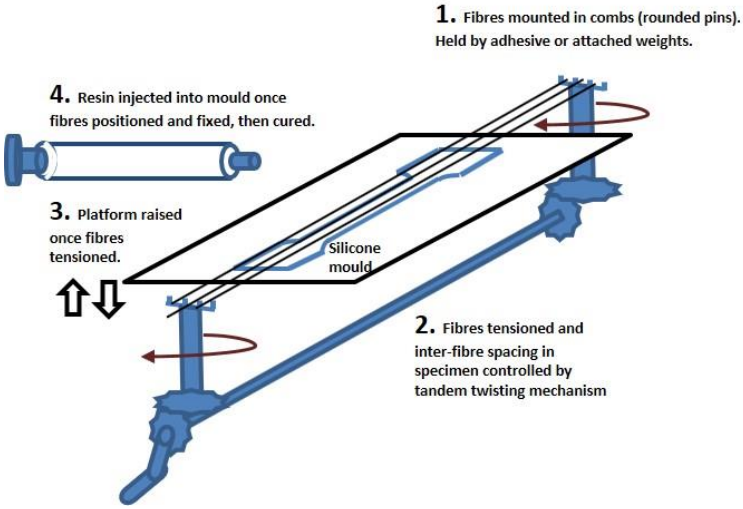

889

890 **Figure 6. Schematic of typical multi-fibre fragmentation embedding system.**

Table

Table 1 Interfibre Stress Transfer Model Predictions for Stress Concentration v. Raman measured values, Grubb et al. [9].

Composite System	Raman Data	Local Load Sharing	Eitan and Wagner	Sector Angle	Overlap
Nicalon/Kevlar	1.45 ± 0.1	1.80	1.26	1.47	1.67
AS4/Kevlar	1.32 ± 0.1	1.28	1.13	1.28	1.28
Fortafil/Kevlar	1.18 ± 0.07	1.25	1.12	1.23	1.24